

UC Berkeley

UC Berkeley Previously Published Works

Title

Fast modulation of visual perception by basal forebrain cholinergic neurons.

Permalink

<https://escholarship.org/uc/item/0dv9c63m>

Journal

Nature neuroscience, 16(12)

ISSN

1097-6256

Authors

Pinto, Lucas
Goard, Michael J
Estandian, Daniel
[et al.](#)

Publication Date

2013-12-01

DOI

10.1038/nn.3552

Peer reviewed



Published in final edited form as:

Nat Neurosci. 2013 December ; 16(12): 1857–1863. doi:10.1038/nn.3552.

Fast Modulation of Visual Perception by Basal Forebrain Cholinergic Neurons

Lucas Pinto^{#1}, Michael J. Goard^{#1,†}, Daniel Estandian¹, Min Xu¹, Alex C. Kwan¹, Seung-Hee Lee¹, Thomas C. Harrison¹, Guoping Feng², and Yang Dan^{1,‡}

¹ Division of Neurobiology, Department of Molecular and Cell Biology, Helen Wills Neuroscience Institute, Howard Hughes Medical Institute, University of California, Berkeley, CA 94720.

² McGovern Institute for Brain Research, Department of Brain and Cognitive Sciences, Massachusetts Institute of Technology, Cambridge, MA 02139.

These authors contributed equally to this work.

Abstract

The basal forebrain provides the primary source of cholinergic input to the cortex, and it plays a crucial role in promoting wakefulness and arousal. However, whether rapid changes in basal forebrain neuron spiking in awake animals can dynamically influence sensory perception is unclear. Here we show that basal forebrain cholinergic neurons rapidly regulate cortical activity and visual perception in awake, behaving mice. Optogenetic activation of the cholinergic neurons or their V1 axon terminals improved performance of a visual discrimination task on a trial-by-trial basis. In V1, basal forebrain activation enhanced visual responses and desynchronized neuronal spiking, which could partly account for the behavioral improvement. Conversely, optogenetic basal forebrain inactivation decreased behavioral performance, synchronized cortical activity and impaired visual responses, indicating the importance of cholinergic activity in normal visual processing. These results underscore the causal role of basal forebrain cholinergic neurons in fast, bidirectional modulation of cortical processing and sensory perception.

The brain state of an animal is modulated on multiple timescales, from the daily sleep-wake cycle to task-dependent changes in vigilance over seconds or minutes. The different brain states are associated with distinct patterns of ensemble neural activity. For example, during quiet wakefulness the cortical local field potential (LFP) exhibits low-frequency, high-

Users may view, print, copy, download and text and data- mine the content in such documents, for the purposes of academic research, subject always to the full Conditions of use: http://www.nature.com/authors/editorial_policies/license.html#terms

‡ To whom correspondence should be addressed. ydan@berkeley.edu.

† Current address: Department of Brain and Cognitive Sciences, Picower Institute for Learning and Memory, Massachusetts Institute of Technology, 77 Massachusetts Avenue, Cambridge, MA, 02139 USA.

AUTHOR CONTRIBUTIONS

L.P. and M.J.G. performed the electrophysiology experiments. L.P., M.J.G. and D.E. performed the behavioral experiments. L.P. and D.E. performed histology. M.X. and A.C.K. developed the behavioral setup. S.-H.L., T.C.H. and L.P. performed the tracing experiments. G.F. provided the *ChAT-ChR2-EYFP* mice. L.P. and M.J.G. analyzed the data. L.P., M.J.G. and Y.D. conceived and designed the experiments and wrote the paper.

COMPETING FINANCIAL INTERESTS

The authors declare no competing financial interests.

Supplementary information is available in the online version of the paper.

voltage oscillations, whereas during running or active sensing the LFP is desynchronized, characterized by high-frequency, low-voltage activity¹⁻³. These states are controlled by internally generated signals², but they strongly influence the processing of sensory inputs¹⁻⁸.

The cholinergic neurons in the basal forebrain constitute an important component of the neuromodulatory system controlling brain states⁹⁻¹¹. These neurons are known to be more active during both wakefulness and rapid-eye-movement (REM) sleep than non-REM sleep¹². During wakefulness, cortical acetylcholine (ACh) concentration also changes in a task-dependent manner on the time scale of seconds¹³. However, the causal relationship between transient increases in cholinergic activity and behavioral performance remains to be demonstrated. Electrical stimulation of the basal forebrain in anesthetized animals causes desynchronization of cortical activity^{14,15}, a hallmark of wakeful and alert brain states, and it enhances cortical responses to sensory stimuli¹⁴⁻¹⁶. However, electrical stimulation also activates numerous non-cholinergic neurons in the basal forebrain^{10,11}, making it difficult to discern the contribution of cholinergic neurons. Furthermore, anesthesia precludes behavioral measurements of sensory perception, and the observed neurophysiological effects may not faithfully reflect the function of basal forebrain activation in awake animals.

In this study, we tested the effects of selective manipulation of basal forebrain cholinergic neuron activity on cortical processing and visual perception in awake mice. We found that channelrhodopsin-2 (ChR2)-mediated activation of the cholinergic neurons improved visual discrimination of the animal and enhanced visual coding by cortical neurons, whereas archaerhodopsin (ARCH)- or halorhodopsin (HALO)-mediated inactivation of these neurons caused the opposite effects. Thus, basal forebrain cholinergic neurons potentially play a powerful role in rapid modulation of sensory processing in the awake brain.

RESULTS

We implanted an optic fiber in the basal forebrain of the transgenic mouse expressing ChR2-EYFP under the choline acetyltransferase (ChAT, a specific marker for cholinergic neurons) promoter¹⁷ (**Fig. 1a,b** and **Supplementary Fig. 1**). Immunohistochemistry confirmed a high degree of co-localization between ChR2-EYFP and ChAT (**Fig. 1c**, 97% of ChR2+ neurons were ChAT+ and 94% of the ChAT+ neurons expressed ChR2). Retrograde tracing with cholera toxin B also confirmed that many cholinergic neurons in the basal forebrain (including those in nucleus basalis, substantia innominata and horizontal limb of the diagonal band of Broca) project their axons to V1 (see Online Methods, **Supplementary Fig. 2**).

Cholinergic activation rapidly desynchronizes cortical LFP

To measure the effect of activating basal forebrain cholinergic neurons on brain state and visual processing, we used a silicon probe to record both LFP and spiking activity from all layers in V1 of awake mice that were head-restrained on a spherical treadmill (see Online Methods, **Fig. 1a**, **Supplementary Movie 1**). We found that light activation of basal forebrain cholinergic neurons reliably desynchronized cortical LFP by reducing the power at low frequencies (1 – 5 Hz) and increasing the power at high frequencies (60 – 100 Hz) (**Fig. 1d,e**, $W_{(13)} = 105$, $P = 1.2 \times 10^{-4}$, Wilcoxon signed rank test, $n = 14$ mice). The effect

occurred rapidly after laser onset (126 ± 21 ms, mean \pm s.e.m., see Materials and Methods) and returned to baseline 691 ± 45 ms after laser offset. This is in contrast to electrical stimulation of basal forebrain, where a 500-ms stimulus induces desynchronization that lasts for 5 – 20s^{14,15}. Thus, basal forebrain cholinergic neurons can modulate cortical LFP on a sub-second to second time scale.

Interestingly, although activating basal forebrain cholinergic neurons caused no significant effect on running speed (**Fig. 1e**, bottom plot, and **Supplementary Fig. 3d**, $W_{(13)} = 32$, $P = 0.62$, Wilcoxon signed rank test, $n = 14$ mice), its effect on LFP depended on the behavioral state of the mouse immediately before laser onset. When the mouse was sitting still (“no run”), the LFP often exhibited large-amplitude low-frequency (< 5 Hz) oscillations (**Supplementary Fig. 3a**) characteristic of quiet wakefulness^{1-3,18}. Basal forebrain activation caused a strong reduction of the low-frequency activity but no clear change at high frequencies (**Supplementary Fig. 3a–c**). When the mouse was running, the baseline LFP showed less low-frequency activity, typical of active behavioral states^{1-3,18}, and basal forebrain activation caused a smaller reduction of low-frequency power but a clear increase at high frequencies. Such an interaction between optogenetic basal forebrain activation and the ongoing behavioral state could be due to additive effects between running- and laser-induced ACh release (e.g., increase in high-frequency power may occur only at high ACh concentrations) or due to interactions between ACh and other inputs to the cortex that are activated by running^{1-3,19}.

Enhancement of behavioral performance

Pharmacological enhancement of cholinergic transmission has been shown to increase attentional modulation^{2,20-22}. We thus tested whether optogenetic activation of basal forebrain cholinergic neurons can improve visual perception. We trained head-fixed mice on a go/no-go task to discriminate between a vertical (target) and a horizontal (non-target) drifting grating (**Fig. 2a**). Once the mice achieved stable performance with gratings at 100% contrast, we varied task difficulty by adjusting the contrast (**Supplementary Movie 2**). Performance was quantified by the discriminability index d' , computed based on the rates of licking in response to the target (hit) and non-target (false alarm) stimuli (see Online Methods). We found that activation of basal forebrain cholinergic neurons improved performance across all contrasts tested (**Fig. 2b,c**, $F_{laser(1,17)} = 7.8$, $P_{laser} = 0.01$; $F_{contrast(2,16)} = 17.2$, $P_{contrast} = 7.1 \times 10^{-6}$; $F_{interaction(2,16)} = 0.41$, $P_{interaction} = 0.66$; two-way repeated-measures ANOVA, $n = 18$). In contrast, laser stimulation had no significant effect in control mice that did not express ChR2 (**Supplementary Fig. 4**, $F_{laser(1,7)} = 1.1$, $P_{laser} = 0.33$, $n = 8$), and the laser-induced increase in d' was significantly higher in the ChAT-ChR2 than the control mice ($F_{laser(1,24)} = 4.0$, $P = 0.05$, two-way ANOVA), indicating that the effect was due to the activation of basal forebrain cholinergic neurons rather than any non-specific effect of the laser light (e.g., through activation of the retinal photoreceptors). The increase in d' was mainly caused by an increase in hit rate (**Fig. 2c**, $F_{laser(1,17)} = 18.6$, $P_{laser} = 4.7 \times 10^{-4}$; $F_{contrast(2,16)} = 25.9$, $P_{contrast} = 1.5 \times 10^{-7}$; $F_{interaction(2,16)} = 1.1$, $P_{interaction} = 0.35$; two-way repeated-measures ANOVA) without significant changes in the false alarm rate ($F_{laser(1,17)} = 0.003$, $P_{laser} = 0.95$). This is consistent with previous lesion studies^{1-8,23,24} and indicates that the improved performance

was not caused by a non-specific increase in lick rate. Note that the increased false alarm rate with contrast (**Fig. 2c**) was not an artifact of the block structure we used in the task, since a similar trend was found when the three contrasts were randomly interleaved on a trial-by-trial basis, not significantly different from the test with block structure (data not shown; $n = 7$; $F_{contrast(2,5)} = 11.4$, $P_{contrast} = 0.002$; $F_{design(1,6)} = 0.02$, $P_{design} = 0.88$; two-way repeated measures ANOVA).

In principle, the laser-induced behavioral improvement could be mediated by increased ACh release in the visual cortex^{9-11,25-28} or in higher brain areas such as the prefrontal cortex (PFC)^{12,13,24,29}. To test the role of the visual cortex, we performed direct optogenetic activation of the cholinergic axons projecting to V1, a widely used approach in optogenetics to isolate the effect of a particular projection (e.g. see refs. 13,30-32). Laser stimulation in V1 significantly reduced low-frequency LFP power (**Supplementary Fig. 5**, $W_{(7)} = 92$, $P = 0.01$, Wilcoxon sing rank test, $n = 8$ mice), similar to the effect found in the somatosensory cortex³⁰. In mice trained to perform visual discrimination (**Fig. 2a**), V1 stimulation also significantly improved performance measured by d' (**Fig. 2d,e**, $F_{laser(1,11)} = 5.9$, $P_{laser} = 0.04$; $F_{contrast(2,10)} = 42.3$, $P_{contrast} = 6.5 \times 10^{-8}$; $F_{interaction(2,10)} = 2.0$, $P_{interaction} = 0.16$; two-way repeated-measures ANOVA, $n = 12$), indicating that optogenetic stimulation within the visual cortex is sufficient to induce a behavioral improvement. Similarly to basal forebrain stimulation, the increase in d' induced by V1 stimulation was due to a significant increase in hit rate (**Fig. 2e**, $F_{laser(1,11)} = 16.1$, $P_{laser} = 0.002$; $F_{contrast(2,10)} = 54.9$, $P_{contrast} = 7.5 \times 10^{-9}$; $F_{interaction(2,10)} = 0.76$, $P_{interaction} = 0.76$) with no significant change in false alarm rate ($F_{laser(1,11)} = 0.17$, $P_{laser} = 0.69$). Unlike basal forebrain stimulation, however, V1 stimulation improved the performance at 20 and 40% contrasts but not at 100% contrast (**Fig. 2d,e**). This suggests that the effect of basal forebrain activation may consist of a V1-mediated perceptual improvement at low contrasts and a non-perceptual component through other pathways (e.g., basal forebrain projection to the PFC^{14-16,26,33}) at high contrasts. Of course, in principle even V1 stimulation could antidromically activate the basal forebrain neurons, which may also project their axon collaterals to other cortical areas. To assess the degree of overlap between the basal forebrain cholinergic neurons projecting to different areas, we performed a dual retrograde tracing experiment by injecting retrobeads of different colors to V1 and other cortical regions. We found very few basal forebrain cholinergic neurons projecting to both V1 and medial PFC or to both V1 and the primary auditory cortex (5% and 6% respectively, **Supplementary Fig. 6**). On the other hand, we found more basal forebrain cells projecting to both V1 and its neighboring higher visual areas (13%, **Supplementary Fig. 6**), leaving open the possibility that ACh release in higher visual areas could also play a role in the behavioral improvement caused by V1 optogenetic stimulation.

Modulation of V1 neuronal activity

To further investigate the neural mechanisms underlying the improved perception, we recorded the visual responses of neurons in all layers of awake mouse V1 (**Fig. 1a**). For the grating stimuli (same as those in the behavioral task, at 20%, 40% and 100% contrasts), activation of basal forebrain cholinergic neurons increased V1 firing rates across all contrasts (**Fig. 3a-c**, $W_{(100)} > 1029$ and $P < 0.001$ for all contrasts, Wilcoxon signed rank test, $n = 101$). Basal forebrain activation also increased the spontaneous firing rate (0%

contrast, $P = 7.4 \times 10^{-4}$), thus causing a shift in the baseline of the contrast response function (**Fig. 3c**), similar to the effect of local application of an ACh agonist in V1^{10,11,27}. We then tested whether these laser-induced increases in V1 responses can improve the discriminability between gratings of different orientations using a receiver operating characteristic (ROC) analysis (see Online Methods). Basal forebrain activation significantly increased the classification performance (**Fig. 3d**, $F_{laser(1,31)} = 6.3$, $P_{laser} = 0.01$; $F_{contrast(2,30)} = 29.3$, $P_{contrast} = 1.1 \times 10^{-9}$; $F_{interaction(2,30)} = 3.7$, $P_{interaction} = 0.03$; two-way repeated-measures ANOVA, $n = 32$ cells), further indicating that the laser-induced changes in V1 activity could at least in part explain the observed improvement in behavioral discrimination.

A previous study in anesthetized rats showed that electrical stimulation of basal forebrain can improve V1 coding of natural scenes by increasing the response reliability of individual neurons and decreasing the correlation between neurons¹⁵. While the decreased correlation was shown to depend on muscarinic ACh receptors in the cortex, whether the improved response reliability was caused by cholinergic transmission was unclear. We thus tested the effects of optogenetic basal forebrain activation on V1 responses to natural stimuli in awake mice (**Fig. 4a**). We found that basal forebrain cholinergic activation caused significant increases in both the firing rate ($W_{(154)} = 4314$, $P = 0.002$, Wilcoxon signed rank test, $n = 155$) and the trial-to-trial response reliability (**Fig. 4b**), as quantified by the decrease of Fano factor (**Fig. 4d**, $W_{(60)} = 1536$, $P = 2.2 \times 10^{-5}$, Wilcoxon signed rank test, $n = 61$). These effects were not caused by basal forebrain activation-induced changes in eye movements (**Supplementary Fig. 7**). Laser stimulation also caused a marked reduction of the coherence between each neuron and the other simultaneously recorded cells at low frequencies, for the responses to both natural movies (**Fig. 4c,e**, $W_{(154)} = 1696$, $P = 7.9 \times 10^{-15}$, Wilcoxon signed rank test, $n = 155$) and drifting gratings (data not shown, $F_{laser(1,39)} = 49.4$, $P_{laser} = 2.0 \times 10^{-8}$, two-way repeated-measures ANOVA, $n = 40$), similar to the effects of ACh application in macaque area MT³⁴.

Local application of ACh receptor antagonists (500 μ M atropine + 3 mM mecamylamine) in V1 significantly weakened laser-induced LFP desynchronization (**Supplementary Fig. 8a,b**; $W_{(7)} = 41$, $P = 0.03$, Wilcoxon sign rank test, $n = 8$ mice), increase in neuronal firing rate (**Supplementary Fig. 8c**; $W_{(60)} = 570$, $P = 0.007$, $n = 61$), and decrease in the coherence between neurons (**Supplementary Fig. 8d**; $W_{(109)} = 967$, $P = 5.0 \times 10^{-10}$, $n = 110$), indicating that these effects are mediated by ACh release within V1. Interestingly, ACh receptor antagonists did not block the laser-induced decrease in Fano factor (**Supplementary Fig. 8e**, $W_{(57)} = 1011$, $P = 0.23$, $n = 58$), consistent with the previous study with electrical stimulation¹⁵. Thus, while specific activation of basal forebrain cholinergic neurons is sufficient to increase cortical response reliability, it is likely mediated by basal forebrain projections to other circuits (e.g., thalamic reticular nucleus^{1-3,18,35}).

Effects of basal forebrain cholinergic inactivation

Basal forebrain cholinergic cells have high tonic firing rates in awake animals^{1-3,12,18}. We wondered whether optogenetic inactivation of these cells could impair cortical coding and visual perception. To selectively inactivate basal forebrain cholinergic neurons, we crossed a

ChAT-Cre driver line with floxed *ARCH-GFP* or floxed *HALO-EYFP* reporter lines. Immunohistochemistry revealed high specificity and efficiency of ARCH/HALO expression (**Fig. 5a**, 93% and 96% of ARCH- and HALO-expressing cells were ChAT+ respectively, and 67% and 82% of ChAT+ neurons expressed the opsins). Since the effects of laser in *ChAT-ARCH* and *ChAT-HALO* mice were similar, they were combined in this study. Laser-induced inactivation of basal forebrain cholinergic neurons (**Supplementary Fig. 1**) led to a significant increase in V1 LFP power at low frequencies (1 – 5 Hz, $t_{(6)} = 2.8$, $P = 0.03$, paired t test, $n = 7$) without affecting the power at high frequencies (60-100 Hz, **Fig. 5b**, $t_{(6)} = 0.89$, $P = 0.41$), opposite to the effect of ChR2-mediated basal forebrain activation. Low-frequency power began increasing at 430 ± 69 ms (mean \pm s.e.m.) after laser onset and returned to baseline at 1.41 ± 0.13 s after laser offset. Basal forebrain cholinergic inactivation also decreased behavioral performance across all contrasts (**Fig. 5c,d**, $F_{laser(1,5)} = 9.0$, $P_{laser} = 0.03$; $F_{contrast(2,4)} = 11.1$, $P_{contrast} = 0.003$; $F_{interaction(2,4)} = 0.16$, $P_{interaction} = 0.85$, two-way repeated-measures ANOVA, $n = 6$ mice), an effect significantly different from the control group (wild-type animals receiving blue laser stimulation, $n = 8$, $F_{laser(1,13)} = 4.4$, $P_{laser} = 0.04$, two-way ANOVA).

At the level of single neurons, basal forebrain inactivation significantly reduced the spontaneous firing rate and the responses to both drifting gratings (**Fig. 6a,d**, $W_{(46)} > 776$ and $P < 0.01$ for all contrasts, Wilcoxon signed rank test, $n = 47$) and natural movies ($W_{(88)} = 3099$, $P = 2.1 \times 10^{-6}$, $n = 89$). The responses to natural movies became less reliable (**Fig. 6b,e**, $W_{(41)} = 74$, $P = 2.4 \times 10^{-6}$, Wilcoxon signed rank test, $n = 42$), and the low-frequency coherence between neurons increased for the responses to both natural movies (**Fig. 6c,f**, $W_{(88)} = 3631$, $P = 2.7 \times 10^{-11}$, Wilcoxon signed rank test, $n = 89$) and drifting gratings ($F_{laser(1,46)} = 13.0$, $P_{laser} = 7.6 \times 10^{-4}$, two-way repeated-measures ANOVA, $n = 47$). Together, these experiments show that optogenetic manipulation of basal forebrain cholinergic neuron activity can bidirectionally modulate brain state and visual cortical processing.

DISCUSSION

Our results show that specific activation of cholinergic neurons in the basal forebrain is sufficient to enhance cortical processing and visual discrimination in awake animals, and this effect occurs rapidly on a sub-second to second time scale. Conversely, optogenetic inactivation of the cholinergic neurons impairs cortical responses and behavioral performance, indicating that the activity of these neurons is necessary for normal visual processing. Thus, the basal forebrain cholinergic neurons could play an immediate, powerful role in activating the cortex and improving sensory processing^{36,37}.

Our results strongly suggest that the basal forebrain activation-induced perceptual improvement is partly mediated by the cholinergic projection to V1 (**Supplementary Fig. 2**). As shown in the ROC analysis, the basal forebrain-induced changes in single neuron responses significantly increased the perceptual limit of the ideal observer (**Fig. 3d**), and the decrease in inter-neuronal correlation (**Fig. 4c,e**) should further improve visual coding at the ensemble level³⁸. Both the increase in firing rate and decrease in correlation depended on cholinergic actions within V1, since they were greatly diminished by local application of

ACh receptor antagonists (**Supplementary Fig. 6**). Furthermore, direct optical activation of cholinergic terminals in V1 was sufficient to improve the behavioral performance at low contrasts (**Fig. 2d,e**), indicating substantial contribution of this pathway. Although in principle stimulation of axon terminals in V1 could cause antidromic activation of the basal forebrain neurons, our dual retrograde tracing experiment showed very little overlap between the basal forebrain cholinergic neurons projecting to V1 and to the PFC (**Supplementary Fig. 6**). This is consistent with a previous study showing that V1- and PFC-projecting neurons in the basal forebrain are segregated and that visual stimulation can evoke ACh release selectively in the visual cortex but not in the PFC²⁶. Thus, even if the V1 stimulation evoked antidromic spiking of the basal forebrain neurons, it would be unlikely to cause cholinergic modulation of the higher brain areas such as the PFC. Of course, in addition to V1, the behavioral effects observed in the basal forebrain activation experiments (**Fig. 2b,c**) could also be mediated by cholinergic projections to other brain structures. For example, we found that the increase in response reliability of V1 neurons was not blocked by local application of ACh receptor antagonists. This is consistent with a previous finding that the increased response reliability induced by electrical stimulation of the basal forebrain also occurs in the lateral geniculate nucleus¹⁵, suggesting involvement of a basal forebrain projection to the thalamus³⁵. Furthermore, basal forebrain projections to higher visual cortices and to other brain areas involved in top-down attentional control, especially the PFC^{13,24,29}, may also contribute to improved behavioral performance.

It is interesting to note that the effects of cholinergic activation we observed – improved task performance, increased spontaneous and visually driven cortical firing rates, improved neuronal response reliability, and decreased inter-neuronal correlation at low frequencies – have all been observed in primates during selective visual attention³⁸⁻⁴². Given such a strong similarity between the effects of basal forebrain cholinergic activation and visual attention at both the behavioral and neuronal levels, cholinergic transmission is likely to be a key component of the neural mechanism for attentional modulation^{13,20-22,24}. In particular, our results are consistent with a recent finding that attentional modulation of neuronal responses and behavioral performance is enhanced by local application of cholinergic agonists in V1²⁰. On the other hand, based on the axonal branching patterns of individual cholinergic neurons⁴³ and their volume transmission of ACh in the cortex⁴⁴, it is unclear if the basal forebrain projections have sufficient spatial specificity to provide the instructive signal for selective attention. Nonetheless, the cholinergic input is likely to play at least a permissive role in attentional modulation.

The basal forebrain cholinergic neurons have long been implicated in crucial brain functions such as arousal, memory, and cortical plasticity, spanning multiple time scales from minutes to hours^{10,11,45-47}. A recent study has shown that variations of ACh concentration in the PFC on the order of seconds correlate with the detection of behaviorally relevant cues¹³. Using cell-type-specific optogenetic manipulation on the same time scale, our experiments establish a causal link between basal forebrain cholinergic neuron activity and enhanced sensory perception in the awake brain.

ONLINE METHODS

Animals and surgery

All procedures were approved by the Animal Care and Use Committee at the University of California, Berkeley. Experiments were performed on adult (2 – 6 months old, 20 – 45 g, both male and female) wild-type (*C57*) and transgenic mice. The animals were housed on a 12/12 h light/dark cycle in cages of up to 5 animals before the implants, and individually after the implants. To activate basal forebrain cholinergic neurons selectively, we used *Chat-ChR2(H134R)-EYFP* mice¹⁷ [line 6, Jackson Laboratories, *B6.Cg-Tg(Chat-COP4*H134R/EYFP)6Gfng/J*, stock number 014546]. To selectively inactivate cholinergic neurons, we crossed *Chat-Cre* mice [Jackson Laboratories, *B6;129S6-Chat<tm1(cre)Lowl>/J*, stock number 006410] with either loxP flanked *ARCH-GFP* [Jackson Laboratories, *129SGt(ROSA)26Sor<tm35.1(CAG-AOP3/GFP)Hze>/J*, stock number 012735] or loxP flanked *HALO-EYFP* [Jackson Laboratories, *B6;129S6-Gt(ROSA)26Sortm39(CAGHOP/EYFP)Hze/J*, stock number 014539] reporter mice. For tracing experiments using CTB we used *Chat-tdTomato* mice obtained by crossing the *Chat-Cre* line with loxP flanked *tdTomato* mice [Jackson Laboratories, *B6.Cg-Gt(ROSA)26Sortm14(CAG-tdTomato)Hze/J*, stock number 007914]. For dual tracing experiments with retrobeads we used wild type (*C57*), *Chat-Cre*, or *GAD2-Cre* mice [Jackson Laboratories, *Gad2tm1(cre/ERT2)Zjh/J*, stock number 010702].

For headplate and cannula implant, mice were anaesthetized with isoflurane (5% induction and 1.5% maintenance) and placed on a stereotaxic frame (David Kopf Instruments). Temperature was kept at 37° C throughout the procedure using a heating pad. After asepsis, the skin was incised to expose the skull and the overlying connective tissue was removed. A reference epidural screw was implanted above the left frontal cortex. A half drilled craniotomy was made to mark the location of the monocular region of the right V1, which was then sealed with a silicone elastomer (Kwik-Cast – World Precision Instruments). We primarily targeted the nucleus basalis, defined as the dorsalmost nucleus in the basal forebrain, lying immediately ventral to the internal capsule and ventromedial to the globus pallidus⁴⁸ (**Supplementary Figs. 1 and 2**). However, it is possible that cholinergic neurons in other basal forebrain nuclei at more ventral locations were also activated by the laser. A cannula with a protective cap (Plastics One) was implanted at 0.5 mm posterior to bregma and 1.8 mm lateral, at a depth of 3.8 mm (0.5 mm above the right nucleus basalis)⁴⁹. Finally, a stainless steel headplate was fixed to the skull using small screws and dental cement. The mice received 2 doses of buprenorphine (0.05 mg/kg, one before surgery and the other 6 – 8 h later) and supplementary analgesia with meloxicam (5 mg/kg) if necessary. They were allowed at least a week of recovery before the experiments.

For single retrograde tracing experiments (**Supplementary Fig. 2**), we exposed the skull over the right V1 and performed a craniotomy (~ 500 µm in diameter, AP: -3.75 mm, ML: 2.0 mm, DV: 500 µm). We then injected 300 – 500 nL of Alexa 488-conjugated cholera toxin subunit B (1 mg/mL CTB-488, Invitrogen) using a borosilicate pipette. Following the injection, the skin was sutured using vicryl. For dual tracing experiments, the surgical procedure was the same as described above, with an additional craniotomy over either PFC

(primarily the prelimbic area, AP: +2.1 mm, ML: 0.3 mm, DV: 1.6 mm), the primary auditory cortex (AP: -2.5 mm, ML: 4.5 mm, DV: 500 μ m) or the medial region of V2 (AP: -2.75 mm, ML: 1.2 mm, DV: 500 μ m). We then injected red or green fluorescent latex microbeads in either area (100 – 200 nL, RetroBeads™, LumaFluor). The animals were euthanized for histology one week after the procedure for CTB tracing and 2-3 days for retrobead tracing.

At the start of each recording session, the mouse was placed on the spherical treadmill⁵⁰ under light isoflurane anesthesia. We removed the silicone elastomer and performed a craniotomy ~300 μ m in diameter over V1, preserving the dura. A laminar silicon probe spanning the depth of the cortex (all layers) was then inserted (~800 μ m long, with up to 32 sites spaced by 50 μ m; NeuroNexus Technologies – models polytrode 1B, 1C or poly2), and the optic fiber was inserted in the cannula to target the ipsilateral basal forebrain. The mouse was removed from anesthesia and allowed to recover for at least 45 min before recording. After the recording session the mouse was euthanized and the brain samples were collected for histology.

To directly activate cholinergic terminals in V1, we implanted the headplate as described above but did not implant the cannula. On the day of the experiment, we performed a craniotomy of ~1 mm in diameter, preserving the dura. The craniotomy was sealed with the silicone elastomer between experimental sessions for mice undergoing behavioral testing.

Optogenetic activation and inactivation

Laser light was delivered to basal forebrain via an optic fiber 200 μ m in diameter (Thorlabs), inserted through and protruding 0.5 mm beyond the implanted cannula. For activation of cortical cholinergic terminals we used a 400 μ m-fiber (Thorlabs) placed ~500 μ m above the dura. For ChR2-mediated activation, we used a 473 nm laser (CrystaLaser or Shanghai Laser and Optics Century Co.) at a power of 1 – 3 mW at the fiber tip for basal forebrain activation and 0.75 – 2 mW for cortical activation experiments. For ARCH-mediated inactivation, we used a 532 nm laser (Shanghai Laser and Optics Century Co.), 15 – 30 mW at fiber tip. For HALO-mediated inactivation, we used a 593 nm laser (CrystaLaser), 15 – 30 mW at the tip. The laser was controlled by TTL pulses generated by either an amplifier (Tucker-Davis Technology – TDT) or a stimulus generator (Master 8, A.M.P.I.). In both behavioral and electrophysiological experiments, we used 5-s long square pulses of laser. Note that in experiments where the optic fiber was targeted at nucleus basalis, some cholinergic neurons in other basal forebrain nuclei could also be activated and thus contribute to the observed effects. As shown in **Supplementary Figure 2**, some of these cholinergic neurons also project to V1.

Visual stimulation

Visual stimuli were generated with a GeForce 7300 Graphics card (NVIDIA) in a PC running custom written software. The mice viewed a gamma-corrected 7" LCD monitor (Xenarc Technologies, maximal luminance: 250cd/m²) with a refresh rate of 75 Hz. The monitor was placed 10 cm away from the left eye. All stimuli were presented in a 50° × 50° region centered at the average receptive field location of all simultaneously recorded units.

Sine-wave gratings used in behavioral and electrophysiology experiments (spatial frequency, 0.04 cycles/degree; temporal frequency, 2Hz) were presented at 20%, 40% or 100% contrast, drifting at either 0° or 90°. For behavior, the drifting grating lasted for 4 s. Laser stimulation lasted for 5 s, from trial start to the end of visual stimulation (**Fig. 2a**). For electrophysiology, each trial started with 1 s of gray screen, followed by 1 s of static grating, followed by drifting grating for 4 s. Laser stimulation lasted for 5 s, from the onset of the static grating to stimulus offset. Baseline firing rates were measured using separate trials with a gray screen (0% contrast). Each experiment consisted of 280 trials (40 trials at each orientation and each contrast, plus 40 trials at 0% contrast), presented in 8 blocks (35 trials per block), with interleaved laser on and laser off blocks.

For natural stimuli, we used three 5-s clips selected from the van Hateren natural movie database⁵¹. Each image was repeated for 3 frames, resulting in an effective frame rate of 25 Hz. Each trial started with 1 s of gray screen, followed by 1 s of the first movie frame, 5 s of movie and 1 s of the last frame. Laser stimulation was concurrent with the movie presentation. Each movie was repeated 60 times in 6 blocks (3 blocks laser on and 3 blocks laser off).

Electrophysiology

We performed multi-site extracellular recordings from awake head-fixed mice that sat on a spherical treadmill⁵⁰. Briefly, an eight-inch Styrofoam ball rested on a metal bowl and was suspended by compressed air to allow the mouse to run with little friction. Running speed was measured with two optical computer mice orthogonally placed at the ball equator using custom-written software in LabVIEW® (National Instruments). The mice were habituated to a similar setup for 1 – 3 days before the recordings. Both spikes and local field potentials (LFP) were recorded using either a Neuralynx Cheetah 27-channel acquisition system (Neuralynx Inc.) or a 32-channel TDT RZ5 (Tucker-Davis Technologies). LFP was band-pass filtered at 1 – 325 Hz and stored at 30 kHz (Neuralynx) or 700 Hz (TDT). Spikes were filtered at 0.6 – 6 kHz and stored as raw voltage traces at 30 kHz (Neuralynx) or 25 kHz (TDT). We used a total of 28 *ChAT-ChR2-EYFP*, 5 *ChAT-ARCH-GFP* and 2 *ChAT-HALO-EYFP* for electrophysiological recordings. We combined the ARCH and HALO data since the results were not statistically different.

Behavior

We trained head-fixed mice on a go/no-go visual discrimination task. The water-restricted mice rested in an acrylic tube located inside a sound-attenuated chamber. Licks were detected by a custom-made infrared lickometer. The animals were typically trained 6 days a week and received all their daily amount of water during the training session (~400 trials, 0.8 – 1 mL). We monitored their weight daily and made sure it did not drop below 85% of the starting value by giving them supplemental water if necessary. Behavioral experiments were carried out during the light cycle, and the experimenter was not blind to group allocation.

Before the visual discrimination task, the mice underwent a period of response shaping and habituation to the apparatus (3 – 5 days), followed by an intermediate conditioning stage in

which they viewed only the “go stimulus” (vertically oriented grating moving rightward) and received a water reward regardless of licking (2 – 4 days). Once they licked consistently during the presentation of the go stimulus, we moved them to the discrimination task with randomly interleaved go and no-go trials. Trial start was signaled by a 500-ms 5 kHz tone, and the grating appeared 1 s after tone onset. The duration of grating stimulus was 4 s, including an initial grace period of 2 s when licking had no consequence followed by a 2-s response window (**Fig. 2a**). We found that introducing this grace period greatly facilitated task learning. In go trials, licking during the response window resulted in an immediate water reward (~4 μ L) through a spout placed close to the animal's mouth. In a no-go trial (horizontally oriented grating moving upward) licking during the response window resulted in an air puff to the cheek (15 – 20 psi, 200 ms) and 8-s timeout period. Inter-trial interval was 3 s. Licking during a go trial was counted as a *hit*, while no lick was counted as a *miss*. In no-go trials, licking was counted as a *false alarm* and no lick as a *correct rejection*. We found that performance was variable across days and subjects, in agreement with previous studies using visual discrimination tasks in mice⁵². Thus, we trained the mice on this task until satisfying the following criteria: for at least 3 consecutive days (1) $d' \geq 0.5$ over the first 100 trials of each training session (indicating that the mouse performed consistently from the beginning of each session), and (2) $d' \geq 1$ over the entire training session or fulfill condition (1) and have reached a limit of 8 weeks of training. These criteria were chosen to ensure that mice were performing above chance, while avoiding excessive overtraining, prior to the experimental manipulations.

Once the mouse reached stable performance defined above (3 – 8 weeks), we started adjusting task difficulty by varying the contrast of the gratings. Different contrasts were presented in different blocks (20 trials/block). Initially we used 6 linearly spaced contrast values (0, 20, 40, 60, 80, and 100%), interleaving every block with a 100% contrast block (2 – 4 days). This was followed by a protocol with blocks of 0% (no stimulus), 20%, 40% or 100% contrast, presented randomly with probability of 1/7, 2/7, 2/7 and 2/7, respectively. We presented fewer 0% contrast blocks because the performance at chance level within these blocks often reduced the animals' motivation to perform the task. The animals were rewarded randomly in these blocks. After 2 – 5 days in this protocol, we introduced laser stimulation at random trials with a 0.5 probability, keeping the contrast block structure. The laser was a square pulse lasting for 5 s, from trial start to visual stimulus offset (**Fig. 2a**). The optic fiber was inserted through the cannula placed above basal forebrain or positioned directly above V1 daily, and these laser stimulation experiments lasted for 1 – 5 days per mouse. We used 18 and 12 *ChAT-ChR2-EYFP* mice for basal forebrain activation and V1 activation experiments, respectively. We excluded another 2 animals from the basal forebrain activation group for having mean $d' < 0$ across contrasts in laser off trials. For basal forebrain inactivation behavioral experiments, we used 1 *ChAT-HALO-EYFP* and 5 *ChAT-ARCH-GFP* mice. The control group consisted of 8 wild types (5 of which were ChR2-negative littermates of *ChAT-ChR2-EYFP* mice).

Histology, immunohistochemistry and retrograde tracing

To confirm the location of the cannula for laser stimulation, after each experiment we inserted a metal wire (200 μ m in diameter) through the cannula to mark the location of the

optic fiber. The animal was deeply anesthetized and euthanized by decapitation. The brain was removed from the skull and fixed in 4% w/v paraformaldehyde (PFA) overnight, followed by cryoprotection with a 30% w/v sucrose solution. The brain was then sectioned in 50- or 70- μ m thick horizontal slices using a cryostat (Leica Microsystems). The slices were mounted with VECTASHIELD® mounting medium with DAPI (Vector Laboratories) and examined with a Microphot-SA fluorescence microscope (Nikon Corp.).

To confirm specific expression of genetically encoded opsins in cholinergic neurons and to label these neurons in dual tracing experiments we performed ChAT immunohistochemistry. The mice were transcardially perfused under deep anesthesia with ~20 – 30 mL of phosphate-buffered saline (PBS) followed by ~20 mL of 4% w/v PFA. Brain samples were kept in PFA overnight, cryoprotected and sliced horizontally with a thickness of 30 μ m (16 μ m for dual retrograde tracing). Samples were thoroughly washed with PBS and incubated for 2 hr with blocking buffer (2% w/v normal goat serum, 0.5% v/v TritonX-100, and 50 mg/mL bovine serum albumin in PBS). The buffer was washed out with PBS and the samples were then incubated overnight at 4° C with primary antibody (1:200 dilution, rabbit Anti-ChAT IgG, catalog # AB143 for opsin co-localization; or goat Anti-ChAT IgG, catalog # AB144P for dual tracing, both from Millipore), washed and incubated for 2 hr at room temperature with the secondary antibody (1:1000 dilution, Alexa Fluor® 594 goat anti-rabbit IgG for opsin co-localization; or Alexa Fluor® 647 donkey anti-goat IgG for dual tracing, both from Invitrogen). This staining protocol is similar to ones previously used in the mouse basal forebrain^{17,30,48}. Slides were mounted using VECTASHIELD® with DAPI. Images were acquired with a 40x oil immersion lens in a Zeiss LSM 780 Confocal Microscope (Carl Zeiss Inc.) and processed in ImageJ (<http://rsbweb.nih.gov/ij/>). Cells were counted in 5 – 7 sections per animal collected randomly from the basal forebrain region of 2 *ChAT-ChR2-EYFP* animals (12 sections, 63 cells) and 2 *ChAT-ARCH-GFP* and 1 *ChAT-HALO-EYFP* animal (17 sections, 182 cells). All cells stained with both DAPI (nuclear) and anti-ChAT antibody (Alexa 594) were considered cholinergic cells, and those stained with DAPI and EYFP+ (or GFP+) were considered ChR2 (or HALO/ARCH)-expressing neurons.

Three *ChAT-tdTomato* mice were used for single V1 retrograde tracing experiments with CTB. They underwent transcardial perfusion, and their brain samples were processed as described above. Brains were sliced into 30- μ m thick coronal sections. Images were acquired with a 20x water immersion lens in a Zeiss LSM 710 Confocal Microscope and processed in ImageJ. Only cells with green fluorescence levels above background and overlap with DAPI staining were considered CTB+. For dual tracing with retrobeads, we used 9 wild type, 2 *ChAT-Cre* and 2 *GAD2-Cre* mice. Brain samples were processed as described above, sliced into 16- μ m thick coronal sections and underwent immunohistochemistry for ChAT. Images were acquired with 10x lens in a Microphot-SA fluorescence microscope. Only cells with green and/or red fluorescence above background and overlap with ChAT staining were counted. Cell counts for dual tracing were performed by 2 different observers and averaged.

Pharmacology

For pharmacological experiments we bath-applied a cocktail containing the muscarinic blocker atropine (500 μ M, Sigma-Aldrich) and the nicotinic blocker mecamylamine (3 mM, Sigma-Aldrich) over the V1 craniotomy. Recordings started 30 – 45 min after drug application, and recovery experiments were carried out 90 – 120 min after drug washout with saline.

Eye tracking

We recorded eye movements in the absence of visual stimulation (gray screen) and during the presentation of natural movies using an infrared camera (QCam 860ML, Premiartek) placed 2 cm away from the animals' eye contralateral to the V1 we recorded from. Images were acquired at a frame rate of 30 Hz and tracking was performed offline. Each frame was converted to a binary image and ellipse fitting was performed to estimate the centre of the pupil position using custom-written software in Matlab.

Data analysis

Spike sorting—Spikes were detected offline with custom-written software. We grouped nearby channels of the silicon probe into groups of 3 or 4 and performed semi-automatic spike sorting using Klusters⁵³. Spike clusters were considered single units if their auto-correlograms had a 2-ms refractory period and their cross-correlograms with other clusters did not have sharp peaks within ± 2 ms of zero lag. We excluded cells with average firing rates < 0.5 Hz. To estimate the cell type we recorded from we computed spike width and peak-to-trough ratio on all average waveforms. Cells fell into two clusters corresponding to putative fast spiking interneurons (~20%) and putative regular spiking cells (~80%)(data not shown). Since there were no systematic differences between the two putative classes regarding the effects of optogenetic manipulation of basal forebrain activity, they are presented together.

Spectral analyses—Time-frequency decomposition of LFP was done with multi-taper analysis⁵⁴ using the chronux toolbox (<http://www.chronux.org/>). LFP was down sampled to 200 Hz before decomposition. We used 5 tapers (time-bandwidth product of 3) and a 1-s sliding window with 50-ms steps. Spectra were averaged across channels. The spectra shown in **Figures 1,5** and **Supplementary Figures 3, 4, 6** were obtained from 30 trials of 5-s square laser pulses (inter-trial interval: 30 s) in which the mice viewed a gray screen. For these analyses, each frequency band was normalized by the average power in the 5-s baseline period preceding basal forebrain stimulation.

We computed the desynchronization ratio as the average power at high frequencies (60 – 100 Hz) divided by the average power at low frequencies (1 – 5 Hz). To estimate the latency of effect onset and offset we calculated the variance of the raw LFP traces for each trial and recording channel over a 250-ms sliding window with 5-ms steps. Onset latency was defined as the first time point at which the average variance was beyond $2 \times$ s.e.m from the mean of the 5-s baseline period preceding laser onset. Offset latency was defined as the first time point after which variance returned to baseline levels for at least 2.5 s. Latency values for each animal were averaged across channels and trials.

For the analysis in **Supplementary Figure 3**, we decomposed the LFP as described above and averaged the power at each frequency over the 5-s windows before and during each trial of laser stimulation. The power in each frequency band was z-scored, and for each 5-s window we averaged the z-scored power between 1 and 5 Hz (low frequency) and between 60 and 100 Hz (high frequency).

Single unit vs. multi-unit coherence was also computed with multi-taper analysis using the same parameters as for LFP. Multi-unit activity was defined as the summed activity of all simultaneously recorded single units except the single unit under comparison. Spiking activity was binned at 1 kHz for all 5 s of natural movie stimulation and for the 4 s of drifting gratings and the average spiking rate was subtracted. Coherence for each single unit vs. multi-unit pair was averaged across trials. Statistical significance of coherence results was calculated on the average across frequencies < 5 Hz. Baseline coherence levels were estimated by performing 5 random trial shuffles for each pair and averaging them. Using an additional correction for differences in firing rate between laser on and laser off conditions by randomly deleting spikes from the condition with the higher firing rate until the firing rates matched yielded very similar results (data not shown).

Single unit responses—For each single unit we computed peri-stimulus time histograms (PSTHs) binned at 10 Hz. For the responses to gratings, we selected units that were significantly driven by either the horizontal or vertical grating (response evoked by 100% contrast grating significantly greater than spontaneous firing rate, measured without basal forebrain stimulation, as assessed by Wilcoxon signed rank test at $P < 0.05$). Using this criterion, 101/153 and 47/77 neurons were selected for further analysis in basal forebrain activation and inactivation experiments, respectively. For the analysis of response reliability (Fano factor) to natural movies, we selected only cells that were driven by the movies, defined as those that had significantly higher within-movie Pearson correlation coefficients than between-movie correlations¹⁵.

To determine if cholinergic activation increases the discriminability of neural responses to different orientations (**Fig. 3d**), we calculated the average neurometric function⁵⁴ under each condition (basal forebrain on, control). For each neuron, the mean spike rate for each single-trial response was used to create response distributions for preferred and non-preferred orientations. The receiver operating characteristic (ROC) was compiled for the distributions using a range of 100 criterion values spanning from the minimum to maximum response. The discriminability of the responses was then calculated by integrating the area under the ROC curve⁵⁵. This analysis was performed separately for each contrast (20%, 40% and 100%) to generate a neurometric function for each condition. Since visual cortical neurons exhibit a wide range of orientation preferences, the majority of recorded neurons did not discriminate well between the two orientations used in the experiments. Thus, in generating an average neurometric function, it was necessary to exclude non-discriminating neurons to reduce variability. For the data shown in **Figure 3d**, we excluded neurons that discriminated with less than 70% accuracy (across contrasts and conditions). The results were similar for discrimination thresholds anywhere in the range 55% - 85% (discrimination thresholds above 85% included too few neurons for robust statistical testing).

Fano factor for the responses to natural movies was calculated as the time average of variance/spike count/mean/spike count using a bin size of 100 ms. Using other bin sizes or Pearson correlation coefficients of between-trial responses as a measure of response reliability yielded qualitatively similar results (data not shown).

Behavioral data—For the analysis of behavioral data, *hit rate* was defined as $\# \text{ hits} / (\# \text{ hits} + \# \text{ misses})$ and *false alarm rate* as $\# \text{ false alarms} / (\# \text{ false alarms} + \# \text{ correct rejections})$. Behavioral performance was summarized as $d' = Z(\text{hit rate}) - Z(\text{false alarm rate})$, where Z is the inverse of the cumulative Gaussian distribution. Individual behavioral sessions were truncated for analysis at the last trial in which the mouse licked.

General statistics—Datasets were tested for normality using the Lilliefors modification of the Kolmogorov-Smirnov test and then compared with the appropriate tests (t or rank tests, all two sided unless stated otherwise). Groups being compared had similar variance. Statistical significance of experiments with factorial design (i.e. involving different contrasts and control/laser conditions) was assessed using two-way repeated-measures ANOVA. Unless otherwise stated, data are presented as mean \pm s.e.m.

Supplementary Material

Refer to Web version on PubMed Central for supplementary material.

Acknowledgments

We thank H.J. Alitto for helpful discussions and E. Rothenberg, J. Cox, G. Pho, S. Zhang, J. Jin, S. Harding-Forrester, C. Oldfield, Y.-C. Kuo, C. Niell, M. Stryker, and M. Sur for technical assistance. This work was supported by NIH R01 EY018861, NSF 22250400-42533 (Y.D.), NIMH RC1-MH088434 (G.F) and a Ruth L. Kirschstein National Research Service Award F31NS059258 from NINDS (M.J.G.).

REFERENCES

1. Crochet S, Petersen CCH. Correlating whisker behavior with membrane potential in barrel cortex of awake mice. *Nat. Neurosci.* 2006; 9:608–610. [PubMed: 16617340]
2. Poulet JFA, Petersen CCH. Internal brain state regulates membrane potential synchrony in barrel cortex of behaving mice. *Nature.* 2008; 454:881–885. [PubMed: 18633351]
3. Niell CM, Stryker MP. Modulation of visual responses by behavioral state in mouse visual cortex. *Neuron.* 2010; 65:472–479. [PubMed: 20188652]
4. Castro-Alamancos MA. Absence of rapid sensory adaptation in neocortex during information processing states. *Neuron.* 2004; 41:455–464. [PubMed: 14766183]
5. Wörgötter F, et al. State-dependent receptive-field restructuring in the visual cortex. *Nature.* 1998; 396:165–168. [PubMed: 9823895]
6. Hasenstaub A, Sachdev RNS, McCormick DA. State changes rapidly modulate cortical neuronal responsiveness. *J. Neurosci.* 2007; 27:9607–9622. [PubMed: 17804621]
7. Marguet SL, Harris KD. State-dependent representation of amplitude-modulated noise stimuli in rat auditory cortex. *J. Neurosci.* 2011; 31:6414–6420. [PubMed: 21525282]
8. Xu S, Jiang W, Poo M-M, Dan Y. Activity recall in a visual cortical ensemble. *Nat. Neurosci.* 2012; 15:449–455. [PubMed: 22267160]
9. Buzsaki G, et al. Nucleus basalis and thalamic control of neocortical activity in the freely moving rat. *J. Neurosci.* 1988; 8:4007–4026. [PubMed: 3183710]
10. Zaborszky L, Duque A. Sleep-wake mechanisms and basal forebrain circuitry. *Front. Biosci.* 2003; 8:d1146–69. [PubMed: 12957822]

11. Jones BE. From waking to sleeping: neuronal and chemical substrates. *Trends Pharmacol. Sci.* 2005; 26:578–586. [PubMed: 16183137]
12. Lee M-G, Hassani OK, Alonso A, Jones BE. Cholinergic basal forebrain neurons burst with theta during waking and paradoxical sleep. *J. Neurosci.* 2005; 25:4365–4369. [PubMed: 15858062]
13. Parikh V, Kozak R, Martinez V, Sarter M. Prefrontal acetylcholine release controls cue detection on multiple timescales. *Neuron.* 2007; 56:141–154. [PubMed: 17920021]
14. Metherate R, Ashe JH. Nucleus basalis stimulation facilitates thalamocortical synaptic transmission in the rat auditory cortex. *Synapse.* 1993; 14:132–143. [PubMed: 8392756]
15. Goard M, Dan Y. Basal forebrain activation enhances cortical coding of natural scenes. *Nat. Neurosci.* 2009; 12:1444–1449. [PubMed: 19801988]
16. Kuo M-C, Rasmusson DD, Dringenberg HC. Input-selective potentiation and rebalancing of primary sensory cortex afferents by endogenous acetylcholine. *Neuroscience.* 2009; 163:430–441. [PubMed: 19531370]
17. Zhao S, et al. Cell type-specific channelrhodopsin-2 transgenic mice for optogenetic dissection of neural circuitry function. *Nat. Methods.* 2011; 8:745–752. [PubMed: 21985008]
18. Bezdudnaya T, et al. Thalamic burst mode and inattention in the awake LGNd. *Neuron.* 2006; 49:421–432. [PubMed: 16446145]
19. Keller GB, Bonhoeffer T, Hübener M. Sensorimotor mismatch signals in primary visual cortex of the behaving mouse. *Neuron.* 2012; 74:809–815. [PubMed: 22681686]
20. Herrero JL, et al. Acetylcholine contributes through muscarinic receptors to attentional modulation in V1. *Nature.* 2008; 454:1110–1114. [PubMed: 18633352]
21. Rokem A, Landau AN, Garg D, Prinzmetal W, Silver MA. Cholinergic enhancement increases the effects of voluntary attention but does not affect involuntary attention. *Neuropsychopharmacology.* 2010; 35:2538–2544. [PubMed: 20811340]
22. Bauer M, et al. Cholinergic Enhancement of Visual Attention and Neural Oscillations in the Human Brain. *Curr. Biol.* 2012; 22:397–402. [PubMed: 22305751]
23. Chiba AA, Bushnell PJ, Oshiro WM, Gallagher M. Selective removal of cholinergic neurons in the basal forebrain alters cued target detection. *Neuroreport.* 1999; 10:3119–3123. [PubMed: 10549833]
24. Sarter M, Hasselmo ME, Bruno JP, Givens B. Unraveling the attentional functions of cortical cholinergic inputs: interactions between signal-driven and cognitive modulation of signal detection. *Brain Res. Rev.* 2005; 48:98–111. [PubMed: 15708630]
25. Sillito AM, Kemp JA. Cholinergic modulation of the functional organization of the cat visual cortex. *Brain Res.* 1983; 289:143–155. [PubMed: 6661640]
26. Laplante F, Morin Y, Quirion R, Vaucher E. Acetylcholine release is elicited in the visual cortex, but not in the prefrontal cortex, by patterned visual stimulation: a dual in vivo microdialysis study with functional correlates in the rat brain. *Neuroscience.* 2005; 132:501–510. [PubMed: 15802200]
27. Disney AA, Aoki C, Hawken MJ. Gain Modulation by Nicotine in Macaque V1. *Neuron.* 2007; 56:701–713. [PubMed: 18031686]
28. Sato H, Hata Y, Masui H, Tsumoto T. A functional role of cholinergic innervation to neurons in the cat visual cortex. *J. Neurophysiol.* 1987; 58:765–780. [PubMed: 3681394]
29. Guillem K, et al. Nicotinic acetylcholine receptor β 2 subunits in the medial prefrontal cortex control attention. *Science.* 2011; 333:888–891. [PubMed: 21836018]
30. Kalmbach A, Hedrick T, Waters J. Selective optogenetic stimulation of cholinergic axons in neocortex. *J. Neurophysiol.* 2012; 107:2008–2019. [PubMed: 22236708]
31. Tye KM, et al. Amygdala circuitry mediating reversible and bidirectional control of anxiety. *Nature.* 2011; 471:358–362. [PubMed: 21389985]
32. Warden MR, et al. A prefrontal cortex-brainstem neuronal projection that controls response to behavioural challenge. *Nature.* 2012; 492:428–432. [PubMed: 23160494]
33. Rye DB, Wainer BH, Mesulam MM, Mufson EJ, Saper CB. Cortical projections arising from the basal forebrain: a study of cholinergic and noncholinergic components employing combined retrograde tracing and immunohistochemical localization of choline acetyltransferase. *Neuroscience.* 1984; 13:627–643. [PubMed: 6527769]

34. Thiele A, Herrero JL, Distler C, Hoffmann KP. Contribution of cholinergic and GABAergic mechanisms to direction tuning, discriminability, response reliability, and neuronal rate correlations in macaque middle temporal area. *J. Neurosci.* 2012; 32:16602–16615. [PubMed: 23175816]
35. Parent A, Pare D, Smith Y, Steriade M. Basal forebrain cholinergic and noncholinergic projections to the thalamus and brainstem in cats and monkeys. *J. Comp. Neurol.* 1988; 277:281–301. [PubMed: 2466060]
36. Yu AJ, Dayan P. Uncertainty, neuromodulation, and attention. *Neuron.* 2005; 46:681–692. [PubMed: 15944135]
37. Ma M, Luo M. Optogenetic Activation of basal forebrain cholinergic neurons modulates neuronal excitability and sensory responses in the main olfactory bulb. *J. Neurosci.* 2012; 32:10105–10116. [PubMed: 22836246]
38. Cohen MR, Maunsell JHR. Attention improves performance primarily by reducing interneuronal correlations. *Nat. Neurosci.* 2009; 12:1594–1600. [PubMed: 19915566]
39. Reynolds JH, Pasternak T, Desimone R. Attention increases sensitivity of V4 neurons. *Neuron.* 2000; 26:703–714. [PubMed: 10896165]
40. Williford T, Maunsell JHR. Effects of spatial attention on contrast response functions in macaque area V4. *J. Neurophysiol.* 2006; 96:40–54. [PubMed: 16772516]
41. Boynton GM. A framework for describing the effects of attention on visual responses. *Vision Res.* 2009; 49:1129–1143. [PubMed: 19038281]
42. Mitchell JF, Sundberg KA, Reynolds JH. Spatial attention decorrelates intrinsic activity fluctuations in macaque area V4. *Neuron.* 2009; 63:879–888. [PubMed: 19778515]
43. Price JL, Stern R. Individual cells in the nucleus basalis–diagonal band complex have restricted axonal projections to the cerebral cortex in the rat. *Brain Res.* 1983; 269:352–356. [PubMed: 6883087]
44. Sarter M, Parikh V, Howe WM. Phasic acetylcholine release and the volume transmission hypothesis: time to move on. *Nat. Rev. Neurosci.* 2009; 10:383–390. [PubMed: 19377503]
45. Kilgard MP, Merzenich MM. Cortical map reorganization enabled by nucleus basalis activity. *Science.* 1998; 279:1714–1718. [PubMed: 9497289]
46. Froemke RC, et al. Long-term modification of cortical synapses improves sensory perception. *Nat. Neurosci.* 2012; 16:79–88. [PubMed: 23178974]
47. Chubykin AA, Roach EB, Bear MF, Shuler MGH. A cholinergic mechanism for reward timing within primary visual cortex. *Neuron.* 2013; 77:723–735. [PubMed: 23439124]
48. Hedrick T, Waters J. Physiological properties of cholinergic and non cholinergic magnocellular neurons in acute slices from adult mouse nucleus basalis. *PLoS ONE.* 2010; 5:e11046. [PubMed: 20548784]
49. Paxinos, G.; Franklin, KBJ. *The mouse brain in stereotaxic coordinates.* Elsevier; San Diego: 2004.
50. Dombeck DA, Khabbaz AN, Collman F, Adelman TL, Tank DW. Imaging large-scale neural activity with cellular resolution in awake, mobile mice. *Neuron.* 2007; 56:43–57. [PubMed: 17920014]
51. van Hateren JH, van der Schaaf A. Independent component filters of natural images compared with simple cells in primary visual cortex. *Proc. Biol. Sci.* 1998; 265:359–366. [PubMed: 9523437]
52. Busse L, et al. The detection of visual contrast in the behaving mouse. *J. Neurosci.* 2011; 31:11351–11361. [PubMed: 21813694]
53. Hazan L, Zugaro M, Buzsáki G. Klusters, NeuroScope, NDManager: a free software suite for neurophysiological data processing and visualization. *J. Neurosci. Methods.* 2006; 155:207–216. [PubMed: 16580733]
54. Mitra, P.; Bokil, H. *Observed Brain Dynamics.* Oxford University Press; New York: 2008.
55. Britten KH, Shadlen MN, Newsome WT, Movshon JA. The analysis of visual motion: a comparison of neuronal and psychophysical performance. *J. Neurosci.* 1992; 12:4745–4765. [PubMed: 1464765]

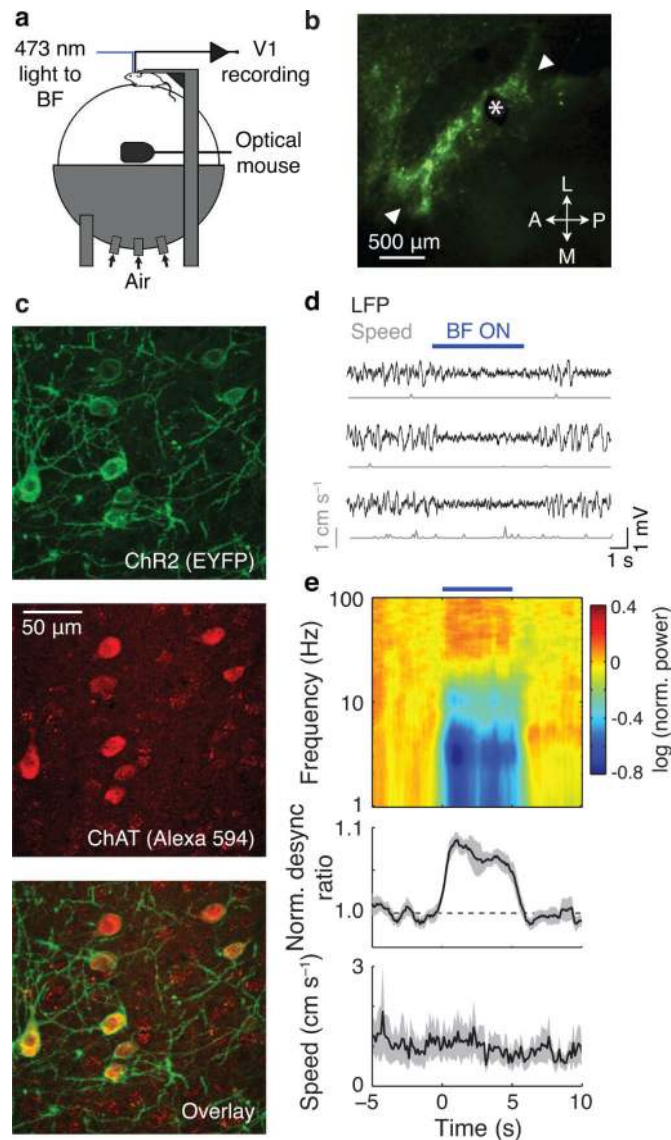
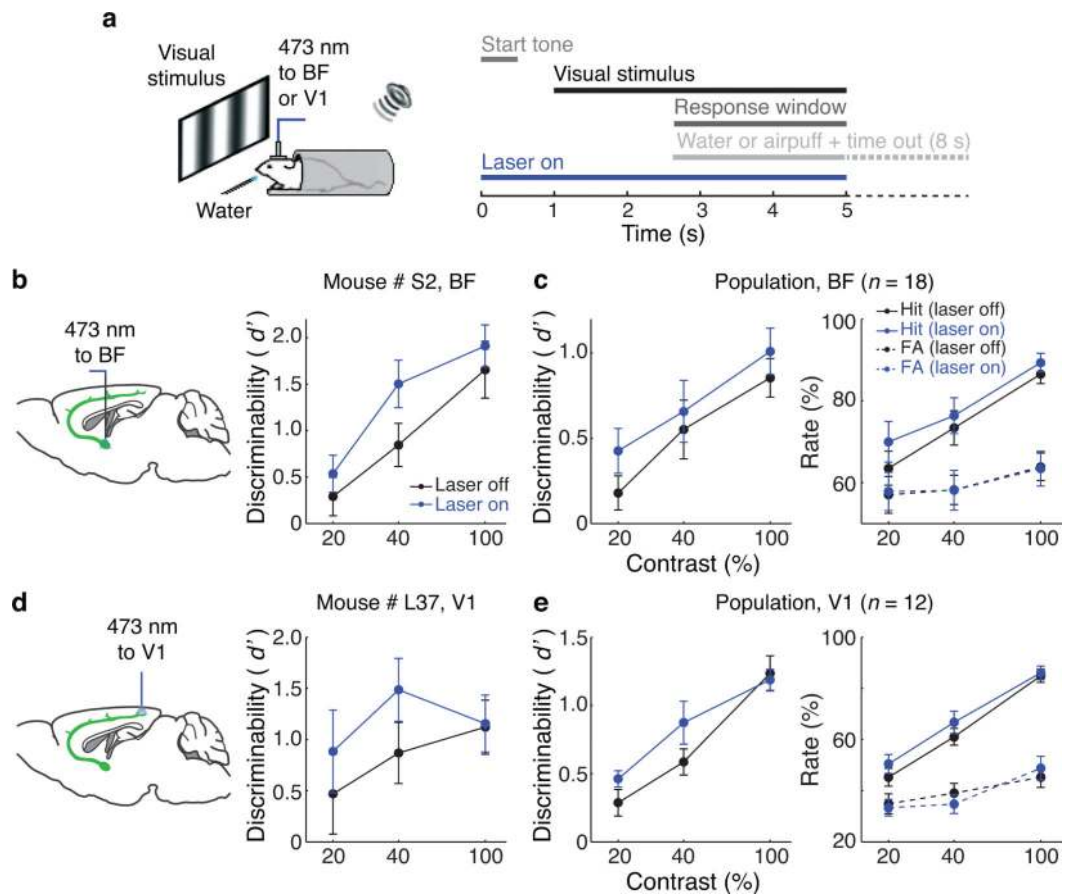


Figure 1. Optogenetic activation of basal forebrain cholinergic neurons in awake mice. **(a)** Schematic illustration of experimental setup. **(b)** Fluorescence microscopy of basal forebrain cholinergic cells expressing ChR2 and EYFP. Asterisk indicates position of optic fiber and arrowheads indicate the posterolateral and anteromedial borders of basal forebrain (nucleus basalis). **(c)** ChAT immunohistochemistry in basal forebrain of a *ChAT-ChR2-EYFP* mouse. **(d)** Example LFP and running speed traces from 3 trials showing the effect of basal forebrain stimulation (blue bar). **(e)** Top: LFP spectra averaged from experiments in 14 different mice, 30 trials/mouse. Blue bar, laser stimulation. Power at each frequency was normalized by the baseline (5-s period preceding laser onset) and color-coded (scale bar on the right). Middle: time course of desynchronization ratio normalized by the baseline. Bottom: average running speed. Gray shading, \pm s.e.m. BF: basal forebrain.

**Figure 2.**

Optogenetic activation of basal forebrain cholinergic neurons or their axons in V1 improved visual discrimination. **(a)** Schematic illustration of behavioral task. **(b)** d' of an example *ChAT-ChR2-EYFP* mouse in laser on and laser off trials for an basal forebrain activation experiment (3 days, 1,048 trials). Error bars, \pm s.e.m. (bootstrap). **(c)** Population average of d' (left) and hit and false alarm (FA) rates (right) in laser on and laser off trials for basal forebrain activation experiments. Error bars, \pm s.e.m. **(d)** d' of an example mouse in laser on and laser off trials for a V1 stimulation experiment (3 days, 614 trials). **(e)** Population average of d' (left) and hit and false alarm rates (right) in laser on and laser off trials for V1 stimulation experiments. BF: basal forebrain, FA: false alarm.

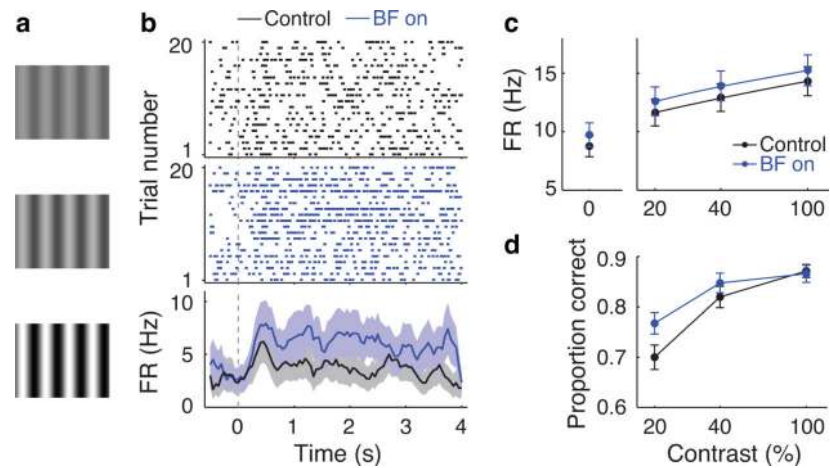


Figure 3.

Effects of basal forebrain activation on V1 neuronal responses to drifting gratings. **(a)** Sine-wave gratings of 20%, 40% and 100% contrasts. **(b)** Top and middle: spike trains of a single unit responding to 100% contrast drifting grating during 20 control (black) and 20 basal forebrain activation (blue) trials. Bottom: corresponding PSTHs for control (black) and basal forebrain activation (blue) trials. Gray dashed line indicates stimulus onset. **(c)** Population average of firing rates vs. contrast for control (black) and basal forebrain activation (blue) trials. **(d)** Classification accuracy of grating orientation from an ROC analysis with and without basal forebrain activation. BF: basal forebrain, FR: firing rate.

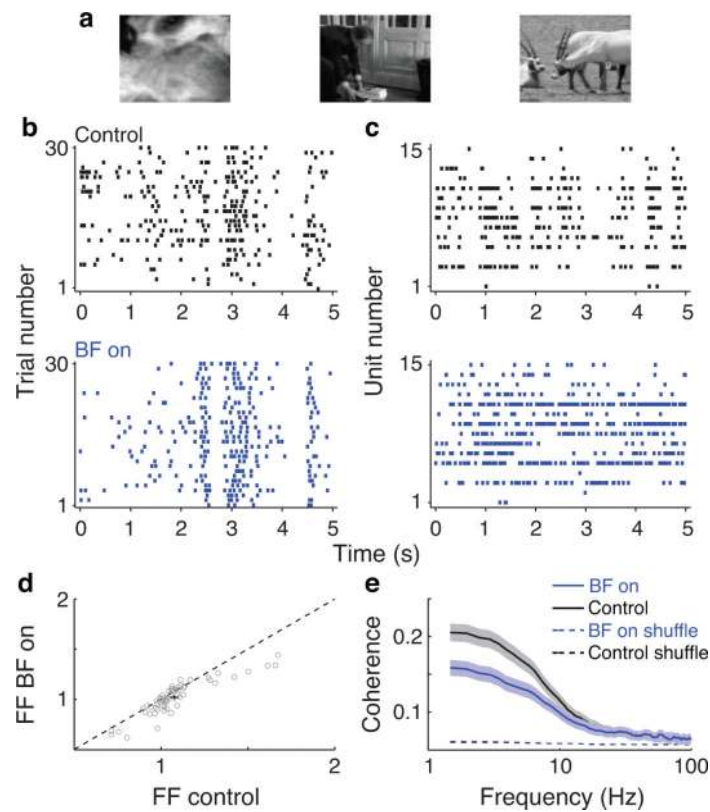
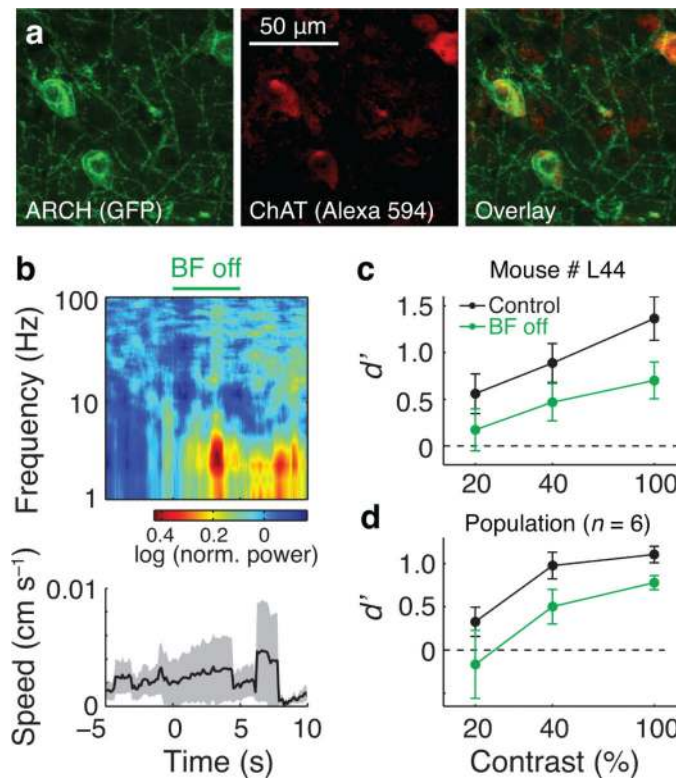


Figure 4.

Effects of basal forebrain activation on V1 neuronal responses to natural movies. **(a)** Example frames of natural movies. **(b)** Spike trains of a single unit in response to 30 repeats of a natural movie during control and basal forebrain activation conditions. **(c)** Spike trains of 15 simultaneously recorded single units in a single trial of natural movie presentation. Note the decrease in correlation between neurons in basal forebrain activation trials. **(d)** Fano factor in response to natural movies for all driven units (open gray circles), basal forebrain on vs. control, measured at a bin size of 100ms. Error bars indicate s.e.m. **(e)** Population average of single unit vs. multi-unit coherence with or without basal forebrain activation. Dashed lines, baseline coherence levels calculated from trial shuffles (blue: basal forebrain on, black: control). Error bars and shaded areas, \pm s.e.m. BF: basal forebrain, FF: Fano factor.

**Figure 5.**

Basal forebrain cholinergic inactivation synchronizes cortical LFP and impairs behavioral performance. (a) ChAT immunohistochemistry in basal forebrain of a *ChAT-ARCH-GFP* mouse. (b) Top: LFP spectra averaged from 7 mice (30 trials/mouse). Green bar, laser stimulation. Power at each frequency was normalized by the baseline and color-coded (scale bar on the right). Bottom: average running speed. Shading, \pm s.e.m. (c) d' of an example *ChAT-ARCH-GFP* mouse in laser on and laser off trials for an basal forebrain inactivation experiment (3 days, 1,101 trials). Error bars, s.e.m. (bootstrap). (d) Population average of d' in laser on and laser off trials for basal forebrain inactivation. Error bars, \pm s.e.m. (green: basal forebrain off, black: control). BF: basal forebrain.

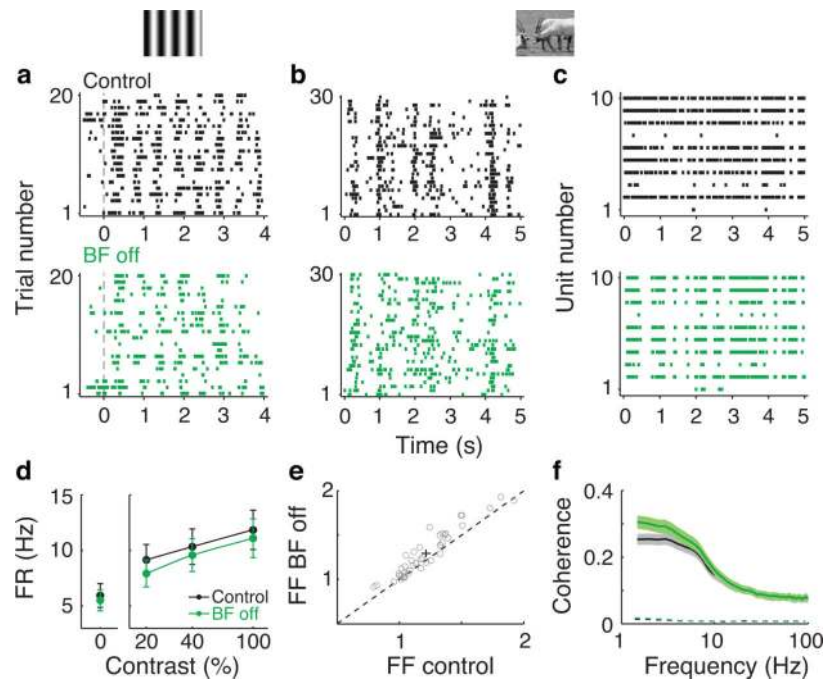


Figure 6.

Effects of optogenetic inactivation of basal forebrain cholinergic cells on V1 responses. **(a)** Spike trains of a simple cell in response to a grating at 100% contrast in 20 control (top panels) and 20 basal forebrain inactivation trials (bottom panels). Note the decrease in firing rate in basal forebrain inactivation trials. Dashed lines indicate stimulus onset. **(b)** Spike trains of an example single unit in response to natural movie stimuli. Note the decrease in trial-to-trial response reliability with basal forebrain inactivation. **(c)** Spike trains of 10 simultaneously recorded single units in a single trial of natural movie presentation (control: top, basal forebrain inactivation: bottom). Note the increase in correlated firing between neurons. **(d)** Firing rate vs. contrast of grating stimuli for control and basal forebrain inactivation trials. **(e)** Fano factor in response to natural movies for all driven units (open gray circles), basal forebrain off vs. control, measured at a bin size of 100 ms. Error bars indicate s.e.m. **(f)** Population average of single unit vs. multi-unit coherence with and without basal forebrain inactivation. Dashed lines, baseline coherence levels calculated from trial shuffles (green: basal forebrain off, black: control). Shading, \pm s.e.m. BF: basal forebrain, FF: Fano factor, FR: firing rate.